

Discovery of Picomolar ABL Kinase Inhibitors Equipotent for Wild Type and T315I Mutant via Structure-Based de Novo Design

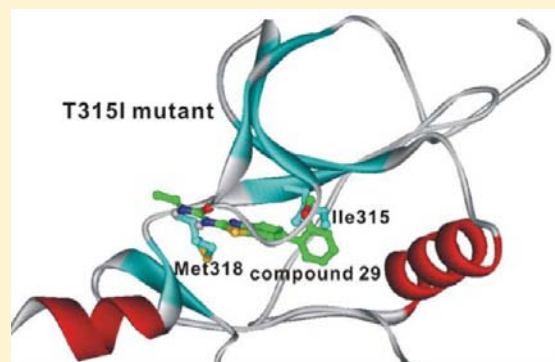
Hwangseo Park,^{*,†} Seunghee Hong,[‡] Jinhee Kim,[‡] and Sungwoo Hong^{*,‡}

[†]Department of Bioscience and Biotechnology, Sejong University, Seoul 143-747, Korea

[‡]Department of Chemistry, Korea Advanced Institute of Science and Technology (KAIST), Daejeon, 305-701, Korea

S Supporting Information

ABSTRACT: Although the constitutively activated break-point cluster region–Abelson (ABL) tyrosine kinase is known to cause chronic myelogenous leukemia (CML), the prevalence of drug-resistant ABL mutants has made it difficult to develop effective anti-CML drugs. With the aim to identify new lead compounds for anti-CML drugs, we carried out a structure-based de novo design using the scoring function improved by implementing an accurate solvation free energy term. This approach led to the identification of ABL inhibitors equipotent for the wild type and the most drug-resistant T315I mutant of ABL at the picomolar level. Decomposition analysis of the binding free energy showed that a decrease in the desolvation cost for binding in the ATP-binding site could be as important as the strengthening of enzyme–inhibitor interaction to enhance the potency of an ABL inhibitor with structural modifications. A similar energetic feature was also observed in free energy perturbation (FEP) calculations. Consistent with the previous experimental and computational studies, the hydrogen bond interactions with the backbone groups of Met318 proved to be the most significant binding forces to stabilize the inhibitors in the ATP-binding sites of the wild type and T315I mutant. The results of molecular dynamics simulations indicated that the dynamic stabilities of the hydrogen bonds between the inhibitors and Met318 should also be considered in designing the potent common inhibitors of the wild-type and T315I mutant of ABL.



INTRODUCTION

The reciprocal translocation between the Abelson gene on chromosome 9 and break-point cluster region gene on chromosome 22 leads to the construction of Philadelphia chromosome. This recombined gene produces the fusion protein (ABL) that is a constitutively active tyrosine kinase and is responsible for the pathogenesis of chronic myelogenous leukemia (CML).¹ Because ABL is involved in most cases of CML, the inhibition of ABL activity offers a novel strategy for the development of therapeutics to treat CML.² Considerable efforts have therefore been devoted to the discovery of small-molecule ABL inhibitors as recently reviewed in a comprehensive fashion.³ These scientific endeavors have identified the potent first-generation ABL inhibitors including imatinib, which was approved for the clinical treatment of CML.⁴

However, CML cells can develop resistance to the first-generation inhibitor drugs by introducing point mutations in the kinase domain of ABL, which has an effect of impeding the binding of inhibitors in the ATP-binding site. At least 100 different point mutations have been identified in CML patients who display resistance to imatinib.⁵ The emergence of drug resistance has complicated the clinical treatment of CML using the first-generation anti-CML drugs and motivated the discovery of new ABL inhibitors with high potency against both the imatinib-resistant mutants and the wild type of ABL.⁶

Included in these second-generation ABL inhibitors are dasatinib,⁷ nilotinib,⁸ bafetinib,⁹ bosutinib,¹⁰ PPY-A,¹¹ tozasertib,¹² danusertib,¹³ AT-9283,¹⁴ and KW-2449.¹⁵ Among the various drug-resistant variants of ABL, T315I mutant has been the most difficult one to deactivate using ATP-competitive ABL inhibitors. This mutation occurs at the gatekeeper site and eliminates a critical hydrogen bond required for tight binding of the inhibitors by changing the geometry of the ATP-binding pocket.¹⁶ Nonetheless, the abundance of structural information about the interactions between the wild-type and mutant ABL kinases and their small-molecule inhibitors has made it possible to discover new anti-CML drugs. Indeed, such structural information has enabled the design of common inhibitors for the wild type and T315I mutant of ABL¹⁷ and has elucidated the mechanism by which the known inhibitors function.¹⁸

Recently, we reported that the antimicrotubule agent, nocodazole in Figure 1, was a common inhibitor of the wild type and T315I mutant of ABL with the associated K_d values of ~ 100 nM.¹⁹ Besides the high inhibitory activities, it has desirable physicochemical properties as a drug candidate and low molecular weight of 301.3 amu. Therefore, it is anticipated to serve as a good inhibitor scaffold from which more potent

Received: December 3, 2012

Published: May 16, 2013

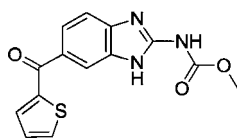


Figure 1. Chemical structure of nocodazole.

common inhibitors can be derivatized. On the basis of the structure-based de novo design and the synthesis of various nocodazole derivatives, we aim in the present study to identify new common inhibitors of wild type and T315I mutant of ABL that can develop into new anti-CML drugs. Computer-aided drug design has not always been successful because of the inaccuracy in the scoring function, which leads to a weak correlation between the computational predictions and experimental results for binding affinities.²⁰ Our de novo design approach is distinguished from others by the implementation of an accurate solvation model in the binding free energy calculations between ABL and the putative ligands. This modification of the scoring function seems to improve the potential for designing the new inhibitors with high activity.²¹ On the basis of docking analysis, molecular dynamics (MD) simulations, and free energy perturbation (FEP) calculations, we also address the energetic and structural features relevant to the stabilization of the newly identified inhibitors in the ATP-binding sites of the wild type and T315I mutant of ABL.

MATERIALS AND METHODS

De Novo Design. The conformation of Asp381-Phe382-Gly383 (DFG) motif in the activation loop is very important for ABL kinase activity because this motif is positioned in proximity to the ATP-binding site. The side chain of Asp381 is directed toward the ATP-binding site in the active conformation to coordinate an ATP-bound Mg²⁺ ion, which is referred to as the “DFG-in” conformation. The side chains of Asp381 and Phe382 swap positions in the inactive (DFG-out) conformation, which leaves the former pointing in opposite direction with respect to the ATP-binding site. The active conformations of the wild type (Figure 2) and T315I mutant of

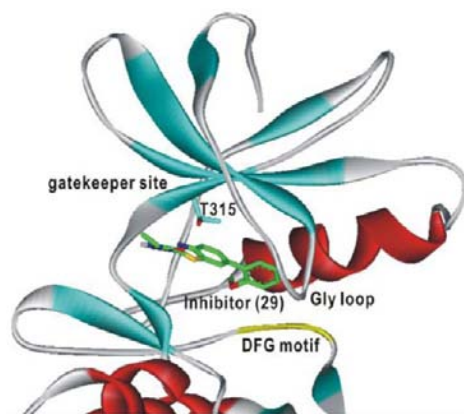


Figure 2. Ribbon representation of ABL in complex with a potent inhibitor (29). The positions of gatekeeper site, Thr315, Gly loop, and DFG motif are indicated.

ABL were selected as the target proteins in this study. We prepared the two receptor models in the “DFG-in” conformation from the X-ray crystal structure of the wild type (residues 229–500, 2.40 Å resolution) in complex with dasatinib (PDB code 2GQG)²² and that of T315I mutant (residues 228–515, 1.95 Å resolution) in complex with PPY-A (PDB code 2QOH).¹¹ These structural models were used

in the de novo design of nocodazole derivatives to identify the common potent inhibitors of the wild type and T315I mutant.

To obtain the all-atom models for the two receptors, hydrogen atoms were added to each protein atom in the wild type and T315I mutant. A special attention was paid to assign the protonation states of the ionizable Asp, Glu, His, and Lys residues in the original X-ray crystal structures. The side chains of Asp and Glu residues were assumed to be neutral if one of their carboxylate oxygens pointed toward a hydrogen-bond accepting group including the backbone aminocarbonyl oxygen at a distance within 3.5 Å, a generally accepted distance limit for a hydrogen bond of moderate strength.²³ Similarly, the lysine side chains were assumed to be protonated unless the NZ atom was in proximity to a hydrogen-bond donating group. The same procedure was also applied to determine the protonation states of ND and NE atoms in His residues.

The structure-based de novo design of new ABL inhibitors was performed in two steps. First, a variety of nocodazole derivatives were generated with the LigBuilder program²⁴ using the calculated ABL-nocodazole and T315I-nocodazole complexes obtained in the previous study.¹⁹ To score the derivatives of a given inhibitor scaffold according to the binding affinity for the target protein, the program employs the empirical binding free energy function including van der Waals, hydrogen bond, electrostatic, and entropic terms.²⁵ As a starting point to generate the nocodazole derivatives, we analyzed the binding pockets in the ATP-binding sites of the wild type and T315I mutant using the POCKET module. The structures of the wild type and T315I mutant in complex with nocodazole were used as the inputs to identify the key interaction residues in the ATP-binding sites. The next step involved the generation of various nocodazole derivatives by applying a genetic algorithm in which the structures were evolved by changing the chemical groups at certain substitution positions with the molecular core being held constant. In this structure-based de novo design, we explored the substituent space on nocodazole at three positions to identify the derivatives with enhanced inhibitory activity against the wild type and T315I mutant of ABL. This could be possible by comparing the calculated binding free energies of the derivatives with respect to the wild type and the mutant. In the first step of de novo design process, the bioavailability rules were also applied to screen the approximately 100 000 derivatives of nocodazole that were expected to have desirable physicochemical properties as a drug candidate.²⁶

Scoring of the Nocodazole Derivatives. Although the effects of ligand solvation have been shown to be critically important in protein–ligand association,²¹ the current scoring function of the LigBuilder program lacks a solvation term. Therefore, the derivatives of nocodazole generated with LigBuilder were further screened with a new binding free energy function constructed by combining an appropriate solvation free energy term to the original scoring function of the AutoDock program.²⁷ This modified scoring function can be expressed in the following form.

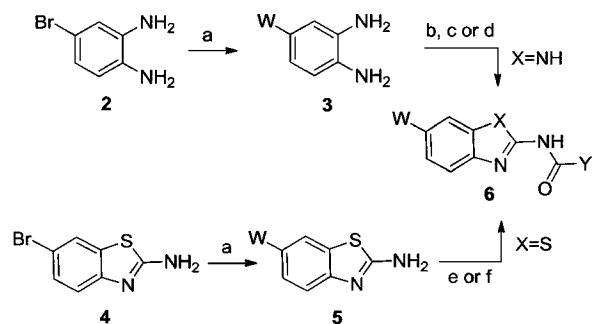
$$\Delta G_{\text{bind}}^{\text{aq}} = W_{\text{vdW}} \sum_{i=1} \sum_{j=1} \left(\frac{A_{ij}}{r_{ij}^{12}} - \frac{B_{ij}}{r_{ij}^6} \right) + W_{\text{hbond}} \sum_{i=1} \sum_{j=1} E(t) \left(\frac{C_{ij}}{r_{ij}^{12}} - \frac{D_{ij}}{r_{ij}^{10}} \right) + W_{\text{elec}} \sum_{i=1} \sum_{j=1} \frac{q_i q_j}{\epsilon(r_{ij}) r_{ij}} + W_{\text{tor}} N_{\text{tor}} + W_{\text{sol}} \sum_{i=1} S_i (O_i^{\text{max}} - \sum_{j \neq i} V_j e^{-r_{ij}^2 / 2\sigma^2}) \quad (1)$$

Here, W_{vdW} , W_{hbond} , W_{elec} , W_{tor} , and W_{sol} are the weighting factors of van der Waals, hydrogen bond, electrostatic interactions, torsional term, and desolvation energy of inhibitors, respectively. r_{ij} represents the interatomic distance, and A_{ij} , B_{ij} , C_{ij} , and D_{ij} are related to the depths of the potential energy well and the equilibrium separations between the protein and ligand atoms. The hydrogen bond term has an additional weighting factor, $E(t)$, representing the angle-dependent directionality. Cubic equation approach was applied to obtain the dielectric constant required in computing the electrostatic interactions between ABL and nocodazole derivatives.²⁸ Gasteiger–Marsili atomic

charges²⁹ were then used for both proteins and ligands to compute the electrostatic interaction energies. In the entropic term, N_{tor} is the number of rotatable bonds in the ligand. In the desolvation term, S_i and V_i are the solvation parameter and the fragmental volume of atom i ,³⁰ respectively, while O_i^{max} stands for the maximum atomic occupancy. In the calculation of molecular solvation free energy of nocodazole derivatives, we used the atomic parameters developed by Choi et al.³¹ This modification of the solvation free energy term seems to have an effect of increasing the accuracy in the scoring function because the underestimation of ligand solvation often leads to the overestimation of the binding affinity of a ligand with many polar atoms.²¹ Indeed, the superiority of this modified scoring function to the previous one was well-appreciated in recent studies for virtual screening of kinase inhibitors.³² Using the binding free energy function in eq 1, the nocodazole derivatives generated with LigBuilder were scored according to the binding affinities for the wild type and T315I mutant of ABL. In this second step of de novo design process, 100 top-ranked derivatives were selected as virtual hits, and the availability of a synthetic path was determined. About thirty of the designed nocodazole derivatives that passed this filter were synthesized and tested for inhibitory activity against the wild type and T315I mutant of ABL.

Chemical Synthesis and Enzyme Assays. The de novo design process identified a variety of promising aromatic ring systems that can be substituted at C6 position of the benzimidazole core. The general synthetic route for the preparation of benzimidazole derivatives is shown in Scheme 1. Functionalization of the C6-position was

Scheme 1. Synthetic Route of Benzimidazole and Benzothiazole Derivatives^a



^aReagents and conditions: (a) Pd(dppf)Cl₂·CH₂Cl₂, arylboronic acid, K₂CO₃, 1,4-dioxane/H₂O = 3:10, 100 °C, 4 h; (b) RCON=C(SMe)-NHCOR (R = OMe (A), NHEt (B)), AcOH/H₂O = 3:1, 100 °C, 5 h; (c) BrCN, MeCN/H₂O, rt, overnight; (d) CDI, DMF, rt, 5 h, then MeNH₂; (e) EtNCO, 1,4-dioxane, 90 °C, 15 h, then H₂O, 100 °C, 3 h; (f) Ac₂O, pyridine, rt, 8 h.

accomplished by direct Suzuki couplings of 4-bromo-1,2-diaminobenzene (2) with corresponding boronic acids, followed by the condensation reaction with appropriate reagents A or B to facilitate the conversions of *o*-phenylenediamines directly to the desired product 6 in high yields. The benzothiazole derivatives were synthesized from 6-bromo-2-aminobenzothiazole 4 because they were expected to be potent ABL inhibitors in the de novo design and docking simulations. After the direct cross-coupling reactions with 4-pyridyl- and phenylboronates under standard coupling conditions, 2-amino group of 5 were further functionalized to either amide or urea groups through the reactions with ethyl isocyanate or anhydride. The synthesized derivatives were then tested to determine the IC₅₀ values against both the wild type and T315I mutant of ABL.³³

MD Simulations. MD simulations of the wild type and T315I mutant of ABL in complex with nocodazole derivatives were carried out using the AMBER program (version 12) with the force field parameters reported by Cornell et al.³⁴ To obtain the potential parameters for nocodazole derivatives unavailable in the force field database, we followed the procedure suggested by Fox and Kollman³⁵

to be consistent with the standard AMBER force field. The starting coordinates of MD simulations were prepared from docking simulations of the nocodazole derivatives in the ATP-binding sites of the wild type and T315I mutant. After the addition of twelve sodium ions for charge neutralization with the AMBER force field parameters, the all-atom models for the wild type and T315I mutant in complex with nocodazole derivatives were immersed in rectangular boxes of dimension 73.8 × 89.6 × 81.7 Å containing 12 904 TIP3P³⁶ water molecules. After 200 cycles of energy minimization to remove the poor steric contacts, we equilibrated the whole system beginning with 20 ps equilibration dynamics of the solvent molecules at 300 K. The next step involved the equilibration of the solute with a fixed configuration of the solvent molecules consecutively at 10, 50, 100, 150, 200, 250, and 300 K for 10 ps at each temperature. Then, the equilibration dynamics of the entire system was performed at 300 K for 100 ps. Following the equilibration procedure, 20.2 ns production dynamics simulations were carried out with periodic boundary conditions in the NPT ensemble. The temperature and pressure were kept at 300 K and 1 atm using Berendsen temperature coupling³⁷ and isotropic molecule-based scaling, respectively. The SHAKE algorithm,³⁸ with a tolerance of 10⁻⁶ Å, was applied to fix all bond lengths involving the hydrogen atom. We used the time step of 2.0 fs and the nonbond-interaction cutoff radius of 12 Å; the trajectory was sampled every 0.4 ps (200-step intervals) for analysis.

FEP Calculations. To further understand the energetic features associated with the inhibition of the wild type and T315I mutant of ABL by nocodazole derivatives, FEP calculations were also carried out based on MD simulations. As the starting structures of these MD-FEP calculations in aqueous solution, we used the final structures of enzyme–inhibitor complexes obtained in the equilibration dynamics. MD-FEP calculations were performed using a thermodynamic cycle-perturbation approach, which is depicted in Figure 3. The change in

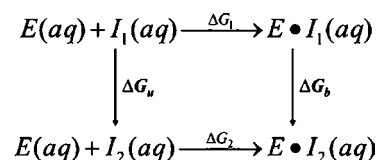


Figure 3. Thermodynamic cycle used in calculating the free energy change in aqueous solution (ΔG_u), that in the ATP-binding site of ABL (ΔG_b), and the difference in binding free energies ($\Delta\Delta G_{\text{bind}}$) between the two inhibitors (I_1 and I_2).

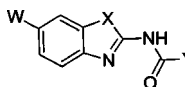
binding free energy ($\Delta\Delta G_{\text{bind}}$) between the two inhibitors can be computed through the nonphysical paths connecting the desired initial and final states. More specifically, this approach enables the calculation of $\Delta\Delta G_{\text{bind}}$ between the two structurally similar inhibitors by computationally simulating the transformation of one into the other. Because the free energy is a state function and, therefore, the sum of all energies in the thermodynamic cycle in Figure 3 is zero, $\Delta\Delta G_{\text{bind}}$ can be expressed as follows.

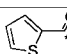
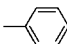
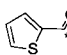
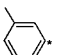
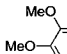
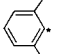
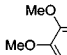
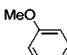
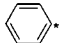
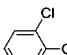
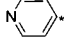
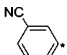
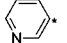
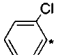
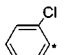
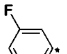
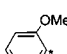
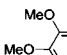
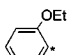
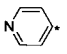
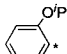
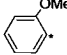
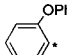
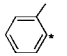
$$\Delta\Delta G_{\text{bind}} = \Delta G_2 - \Delta G_1 = \Delta G_b - \Delta G_u \quad (2)$$

Here, ΔG_1 and ΔG_2 refer to the binding free energies of inhibitors I_1 and I_2 , respectively, and ΔG_u and ΔG_b to the free energies associated with the structural transformation of I_1 into I_2 in aqueous solution and in the ATP-binding site of ABL.

To determine the $\Delta\Delta G_{\text{bind}}$ value between I_1 and I_2 , therefore, the free energy changes in transforming I_1 into I_2 should be calculated both in aqueous solution and in the ATP-binding site of ABL. The free energy change for converting I_1 into I_2 was computed by perturbing the Hamiltonian of I_1 (initial state) into that of I_2 (final state). This transformation could be accomplished through the parametrization of the terms comprising the interaction potentials of the system with the change of a state variable (λ) that mapped onto reactant ($\lambda = 0$) and product ($\lambda = 1$) states. The total free energy change for the mutation from the initial to the final state was then computed by summing the incremental free energy changes over several windows visited by λ as it

Table 1. Structures and Inhibitory Activities of Representative Nocodazole Derivatives



	W ^a	X	Y	IC ₅₀ (nM)		W ^a	X	Y	IC ₅₀ (nM)		
				wild type	T315I				wild type	T315I	
1		NH	OCH ₃	210	640	19		NH	NHCH ₂ CH ₃	3720	699
7		NH	NHCH ₂ CH ₃	8.95	23.2	20		NH	NHCH ₂ CH ₃	25.1	139
8		NH	OCH ₃	>10000	>10000	21		NH	NHCH ₂ CH ₃	15.2	45.2
9		NH	NHCH ₂ CH ₃	110	2000	22		NH	NHCH ₂ CH ₃	136	182
10		NH	NHCH ₂ CH ₃	70.2	43.7	23		NH	NHCH ₂ CH ₃	45.5	239
11		NH	NHCH ₂ CH ₃	70	200	24		NH	NHCH ₂ CH ₃	146	953
12		NH	NHCH ₂ CH ₃	934	1390	25		NH	NHCH ₂ CH ₃	22.7	17.1
13		NH	NHCH ₂ CH ₃	12.9	21.4	26		NH	NHCH ₂ CH ₃	12.6	23.2
14		NH	NHCH ₂ CH ₃	18.8	6.22	27		S	NHCH ₂ CH ₃	1.99	21.1
15		NH	NHCH ₂ CH ₃	1.61	2.28	28		S	NHCH ₂ CH ₃	1.12	2.01
16		NH	NHCH ₂ CH ₃	6.77	46.7	29		S	NHCH ₂ CH ₃	0.06	0.11
17		NH	NHCH ₂ CH ₃	145	1480						
18		NH	NHCH ₂ CH ₃	7.78	16.9						

^aAsterisk indicates the atom attached to the position of substitution.

changed from 0 to 1. Starting from the initial structures, we performed 1680 ps of perturbation for a selected pair of nocodazole derivatives. Each perturbation consisted of 21 windows with 40 000 steps of equilibration and 40 000 steps of data collection. We used the time step of 1 fs and the nonbond-interaction cutoff radius of 12 Å. A doublewise sampling procedure was performed for all of the structural transformations, and the reported results were based on the averages from the backward and forward simulations. As a rough estimation of the statistical error, we used half the difference between the absolute values of forward and reverse free energy changes, and the error in $\Delta\Delta G_{\text{bind}}$ was calculated as the square root of the sum of the squares of the individual errors in ΔG_{a} and ΔG_{b} .

RESULTS AND DISCUSSION

Inhibitory Activities of Nocodazole Derivatives.

Among the nocodazole derivatives prepared and tested for the inhibitory activity, more than ten compounds were found to have a high potency against both the wild type and T315I mutant of ABL at the submicromolar level. Table 1 lists the structures and IC₅₀ values of the representative inhibitors. Most nocodazole derivatives exhibit a higher potency against the wild type than against T315I mutant. This result is consistent with the difficulty associated with achieving a high inhibitory activity for T315I mutant.³⁹ We note that the change of the terminal

methoxy group in nocodazole (**1**) to ethylamine in **7** leads to more than 20-fold increase in inhibitory activity both for the wild type and for T315I mutant. This significant enhancement of potency is most likely to stem from the strengthening of the hydrogen bonds with protein groups because the terminal carbamate group in **1** was found to establish multiple hydrogen bonds at the entrance of ATP-binding site of ABL.¹⁹ In contrast, the substitution of 3,4-dimethoxybenzene in **8** for the thiophene-2-one group in **1** leads to the loss of potency. However, the inhibitory activity can be recovered by the additional replacement of terminal methoxy group with ethylamine in **9**, which confirms that the formation of strong hydrogen bonds in the ATP-binding site are critically important for the effective inhibition of the wild type and T315I mutant ABL. The high inhibitory activities of **14** and **15** toward both the wild type and T315I mutant indicate that 2-methoxyphenyl and 2-ethoxyphenyl groups can serve as the best substituents at W position of the inhibitor scaffold (Table 1). Most remarkably, the change of the central aromatic group from benzimidazole in **9** and **11** to benzothiazole in **27** and **28** leads to the increase in the inhibitory activity by a factor of 50–100. The combination of 2-methoxybenzene group, benzothiazole core, and ethylamine moiety at the three substitution positions

yields the most potent inhibitor (**29**) with picomolar activity. Judging from the exceptionally high inhibitory activities against both the wild type and T315I mutant, **29** deserves consideration for further investigation toward the development of new anti-CML medicines.

Binding Mode Analysis of the Newly Identified Inhibitors. To obtain some energetic and structural insight into the inhibitory mechanisms of the newly identified common inhibitors of the wild type and T315I mutant of ABL, their binding modes in the ATP-binding sites were investigated using the modified AutoDock scoring function. The calculated binding modes of **1**, **7**, and **9** with respect to the wild type and T315I mutant are compared in Figure 4. All three

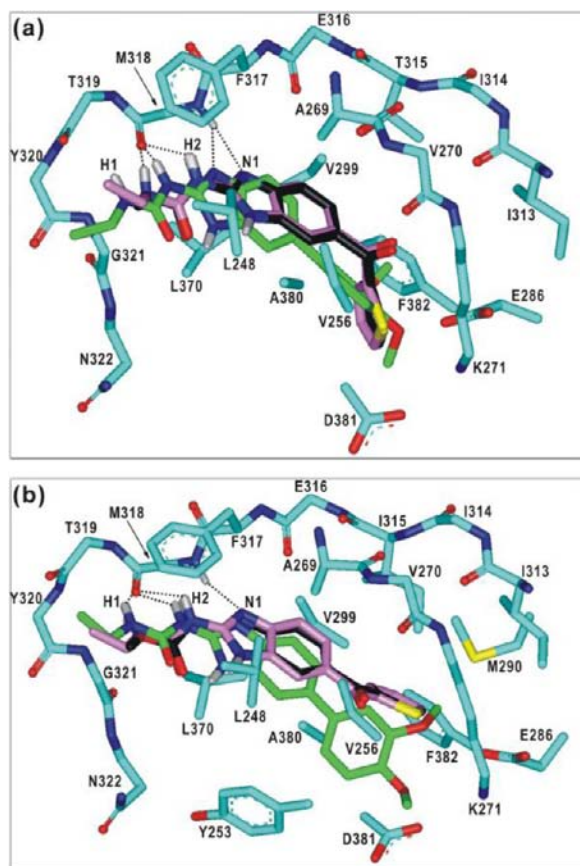


Figure 4. Calculated binding modes of **1**, **7**, and **9** in the ATP-binding sites of (a) wild type and (b) T315I mutant of ABL. Carbon atoms of ABL, **1**, **7**, and **9** are indicated in cyan, black, pink, and green, respectively. Each dotted line indicates a hydrogen bond.

inhibitors appear to form close contacts with residues Leu248–Tyr256, Ile313–Asn322, and Ala269–Lys271, which belong to the Gly loop, the gatekeeper site, and a β -sheet in the N-terminal domain, respectively. It is a common structural feature in the calculated binding modes of three inhibitors for the wild type and T315I mutant that a nitrogen in the imidazole ring (N1) and the adjacent amidic hydrogen (H2) form a hydrogen bond with the backbone amidic hydrogen and the amino-carbonyl oxygen of Met318, respectively. This is consistent with the previous X-ray crystallographic studies on ABL-inhibitor interactions in which the formation of multiple hydrogen bonds with the backbone groups of Met318 was shown to be necessary for tight binding of the inhibitors in the ATP-binding site.^{11,22}

It is interesting to note that the number of hydrogen bonds increases from two to three as the inhibitor changes from **1** to **7** both for the wild type and for T315I mutant. This trend can be attributed to the change of the terminal methoxy group in **1** to the ethylamine group that can establish an additional hydrogen bond with the backbone aminocarbonyl oxygen of Met318. This strengthening of hydrogen bond interactions is apparently responsible for the higher inhibitory activities of **7** than **1** toward the wild type and T315I mutant. In the calculated structure of ABL-**9** complex, however, only two hydrogen bonds are established with Met318 due to the disappearance of a hydrogen bond between the aminocarbonyl oxygen of Met318 and the hydrogen atom (H1) on the terminal ethylamine moiety of **9**. As can be inferred from the superimposed structures of **1**, **7**, and **9** in Figure 4a, the absence of such a hydrogen bond seems to be caused by the enlargement of the terminal aromatic group from thiophene-2-one group to 3,4-dimethoxybenzene, which induces the positional shift of the inhibitor from the ATP-binding site to bulk solvent. This indicates that the size of terminal aromatic group should be restricted for the optimal inhibitory activity of nocodazole derivatives. Besides the hydrogen bond interactions, the inhibitors can be further stabilized in the ATP-binding sites via the hydrophobic interactions of their nonpolar groups with the side chains of Leu248, Tyr253, Val256, Ala269, Val299, Phe317, Leu370, Ala380, and Phe382. Overall, the structural features identified in docking simulations indicate that the high inhibitory activities of certain nocodazole derivatives against the wild-type and T315I mutant of ABL stem from the multiple hydrogen bonds and hydrophobic interactions established simultaneously in the ATP-binding sites.

Despite several similarities in binding modes toward the wild-type and T315I mutant, some differences are also observed both in hydrogen bond and in hydrophobic interactions. For example, two additional residues (Met290 and Ile315) are found at the interface of van der Waals contacts between the inhibitors and T315I mutant (Figure 4b), indicating that the hydrophobic interactions must be established in the stronger fashion in T315I-inhibitor than in ABL-inhibitor complexes. On the other hand, the hydrogen bonds between Met318 and the inhibitors get weaker with the change of the receptor from the wild type to T315I mutant. The two N–H \cdots N hydrogen bond distances increase from, respectively, 2.06 Å and 2.07 Å in ABL-**1** and ABL-**7** complexes to 2.30 Å and 2.20 Å in T315I-**1** and T315I-**7** complexes, respectively. The strengthening of hydrophobic interactions in T315I-inhibitor complexes is likely to be insufficient to compensate for the weakening of the hydrogen bonds because **1** and **7** have a lower inhibitory activity for T315I mutant than for the wild type (Table 1). Unlike the binding mode in ABL-**9** complex, all three hydrogen bonds are established in T315I-**9** complex in a stable form as in T315I-**7** complex. Nonetheless, the binding mode of **9** in the ATP-binding site of T315I mutant differs significantly from those of **1** and **7** in that 3,4-dimethoxybenzene group of **9** stays distant from the ATP-binding site and points toward the DFG motif located at the top of C-terminal domain. As can be seen in Figure 4b, 3,4-dimethoxyphenyl moiety of **9** is less stabilized in the ATP-binding site than thiophene-2-one group of **1** and **7** because of the increase in repulsive interactions with the side

chain of Ile315, which prevents a bulky group from being accommodated in the ATP-binding site. Such a difficulty in the stabilization of terminal 3,4-dimethoxybenzene group in the ATP-binding site may be an explanation for the significant decrease in the inhibitory activity for T315I mutant in going from **1** and **7** to **9**. The importance of reducing the repulsive interactions in designing the T315I mutant inhibitors was also implicated in recent X-ray crystallographic studies of ABL in complex with bosutinib.⁴⁰

To examine the dynamic stabilities of the proposed binding modes shown in Figure 4, we carried out 20 ns MD simulations of the wild type and T315I mutant of ABL in complex with **1**, **7**, and **9**. Compared in Figure 5 are the time evolutions of the

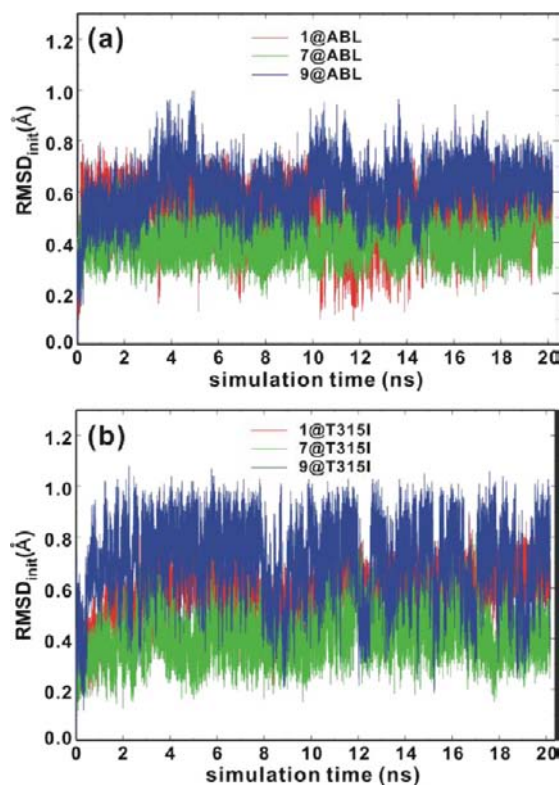


Figure 5. Time evolutions of the root-mean-square deviation ($\text{RMSD}_{\text{init}}$) values for heavy atoms of **1**, **7**, and **9** in the ATP-binding sites of (a) wild type and (b) T315I mutant of ABL.

root-mean-square deviations ($\text{RMSD}_{\text{init}}$) for the heavy atoms of **1**, **7**, and **9** in the ATP-binding sites of the wild type and T315I mutant of ABL. The $\text{RMSD}_{\text{init}}$ values of the three inhibitors in ABL-**1**, ABL-**7**, and ABL-**9** complexes remain lower than those in T315I-**1**, T315I-**7**, and T315I-**9** complexes in the majority of simulation time, which indicates that the inhibitors bind more tightly in the ATP-binding site of the wild type than in that of T315I mutant. This is consistent with a little higher inhibitory activities of **1**, **7**, and **9** against the wild type than the mutant (Table 1). It is also noteworthy that the $\text{RMSD}_{\text{init}}$ values fall into 0.8 Å in most enzyme–inhibitor complexes with the average values of 0.41–0.61 Å except for the T315I-**9** complex, which indicates an insignificant positional shift of the inhibitors during the entire course of simulation. On the other hand, **9** exhibits a high motional amplitude in the ATP-binding site of T315I mutant with the average $\text{RMSD}_{\text{init}}$ value of 0.71 Å (Figure 5b). This dynamic instability may be invoked to explain the low inhibitory activity of **9** against T315I mutant (Table 1)

and the relatively unfavorable interaction in the ATP-binding site predicted in docking simulations (Figure 4b).

Figure 6 shows the calculated binding modes **11**, **28**, and **29** in the ATP-binding sites of the wild type and T315I mutant of

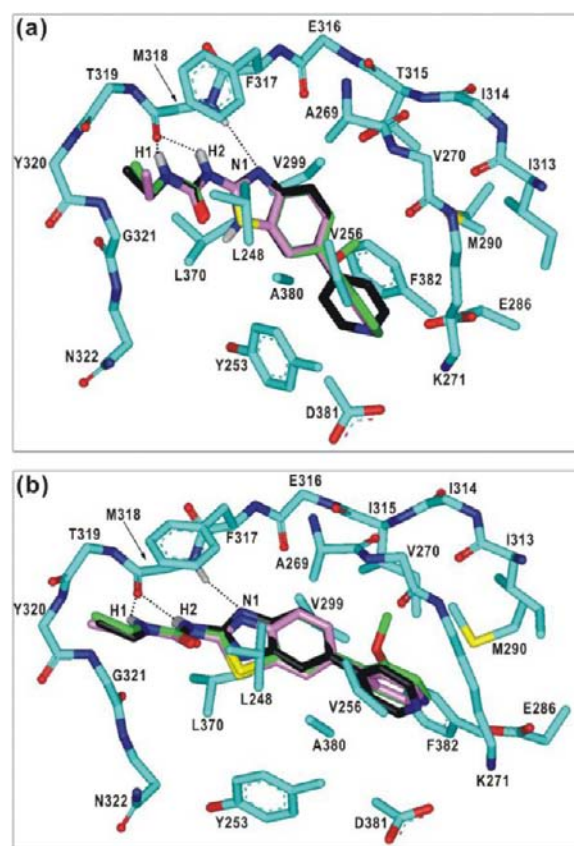


Figure 6. Calculated binding modes of **11**, **28**, and **29** in the ATP-binding sites of (a) wild type and (b) T315I mutant of ABL. Carbon atoms of ABL, **11**, **28**, and **29** are indicated in cyan, black, pink, and green, respectively. Each dotted line indicates a hydrogen bond.

ABL. The overall structural features derived from docking simulations confirm that the high inhibitory activities of nocodazole derivatives toward the wild type and T315I mutant stem from the multiple hydrogen bonds and hydrophobic interactions established simultaneously in the ATP-binding site. As a consequence of the change of the aromatic group in *W* position from 3,4-dimethoxybenzene in **9** to pyridine in **11**, the third hydrogen bond is established in a stable form between the terminal ethylamine group of the inhibitor and the amino-carbonyl oxygen of Met318 of the wild type (Figure 6a). This is consistent with the higher inhibitory activity of **11** than **9** with respect to the wild type (Table 1). The substitution of pyridine in **11** for 3,4-dimethoxybenzene in **9** has also an effect of stabilizing the inhibitor in the ATP binding site of T315I mutant by reducing the repulsive interactions with the side chain of Ile315. This feature may account for the 10-fold increase in the inhibitory activity of **9** over **11** with respect to T315I mutant. Although the docking simulations of **1**, **7**, and **9** provided some insight into the relative potencies observed over the series, the significant differences in IC_{50} values of **11**, **28**, and **29** are difficult to explain because their calculated binding modes with respect to the wild type and T315I mutant are quite similar. For example, the urea moiety common in all three inhibitors establishes three hydrogen bonds with backbone

groups of Met318 at the entrance of ATP-binding site while their nonpolar groups are stabilized at the ATP-binding site by hydrophobic interactions with the side chains of Leu248, Tyr253, Val256, Ala269, Met290, Val299, Ile315, Phe317, Leu370, Ala380, and Phe382. Therefore, further energetic and structural analyses were performed to elucidate the differences in inhibitory activities of the derivatives with similar binding modes.

Decomposition Analysis of Binding Free Energy. We now turn to the energetic features associated with binding of the newly identified inhibitors in the ATP-binding sites of the wild type and T315I mutant of ABL. Table 2 lists the calculated

Table 2. Calculated Binding Free Energies of ABL Inhibitors^a

compd	ΔG_b^{gas}		ΔG^{sol}	ΔG_b^{aq}	
	wild type	T315I		wild type	T315I
1	-20.9	-20.7	-12.9	-8.0	-7.8
7	-23.2	-23.5	-13.9	-9.3	-9.6
9	-22.6	-22.0	-16.2	-6.4	-5.8
11	-23.3	-23.2	-15.3	-8.0	-7.9
28	-23.1	-23.3	-12.5	-10.6	-10.8
29	-23.8	-23.5	-12.8	-11.0	-10.7

^aCalculated binding free energy in the gas phase (ΔG_b^{gas}), solvation free energy (ΔG^{sol}), and binding free energy in solution (ΔG_b^{aq}) of the selected inhibitors with respect to the wild type and T315I mutant of ABL. The ΔG_b^{aq} values indicate the final binding free energies for the best binding configurations. All energy values are given in kcal/mol.

binding free energies in solution and solvation free energies of the six inhibitors mentioned above. Bearing in mind that the binding free energy of a protein–ligand complex in aqueous solution (ΔG_b^{aq}) may be approximated as the difference between that in the gas phase (ΔG_b^{gas}) and the solvation free energy of the ligand (ΔG^{sol}), we computed the two energy components separately to estimate their relative contributions to ΔG_b^{aq} . When the two energy components for the six inhibitors are compared, it follows immediately that ΔG^{sol} values correspond to 50–70% of ΔG_b^{gas} and are larger in magnitude than ΔG_b^{aq} . This indicates that the solvation free energy should be considered as a significant energy component in the scoring function for the binding affinities of ABL inhibitors. To enhance the potency of an ABL inhibitor with structural modifications, therefore, the resulting increase in the strength of enzyme–inhibitor interactions should be sufficient to surmount the increased stabilization in solution.

The calculated binding free energies of the six inhibitors compare reasonably well with their relative inhibitory activities and structural features found in docking simulations. For example, ΔG_b^{gas} and ΔG^{sol} values of 7 are lower than those of 1 by 2.3–2.8 and 1.0 kcal/mol, respectively, which leads to the lowering of ΔG_b^{aq} in going from 1 to 7. The larger decrease in ΔG_b^{gas} than ΔG^{sol} indicates that the strengthening of enzyme–inhibitor interactions because of the substitution of ethylamine group in 7 for the terminal methoxy group in 1 should be sufficient to overcome the increase in desolvation cost for the enzyme–inhibitor complex formation. This can be invoked to explain the higher inhibitory activity of 7 than 1. The enlargement of the thiophene-2-one group in 7 to 3,4-dimethoxybenzene in 9 leads to the increase and the decrease in ΔG_b^{gas} and ΔG^{sol} values, respectively, which indicates the weakening of enzyme–inhibitor interactions and the increase in

desolvation cost. For this reason, the ΔG_b^{aq} values of 9 associated with the binding in the ATP-binding sites of the wild type and T315I mutant become less favorable than the corresponding values of 7 by 2.9 and 3.8 kcal/mol, respectively, which is consistent with more than 10-fold decrease in inhibitory activity (Table 1). As can be inferred from the decrease in ΔG_b^{gas} and the increase in ΔG^{sol} values in going from 9 to 11, the change of 3,4-dimethoxybenzene in 9 to pyridine in 11 enhances the inhibitory activity by strengthening the enzyme–inhibitor interactions and by reducing the desolvation cost for complexation.

With respect to the importance of the hydrogen bonds with the backbone groups of Met318, we note that ΔG_b^{gas} values become more favorable from -20.9 and -20.7 kcal/mol in ABL-1 and T315I-1 complexes to -23.2 and -23.5 kcal/mol in ABL-7 and T315I-7 complexes, respectively. Because the calculated binding modes of the two inhibitors are very similar except for the number of hydrogen bonds with Met318 (Figure 4), the gain of extra stabilization energy by 2.3 (wild type) and 2.8 kcal/mol (T315I mutant) with the change of the inhibitor from 1 to 7 can be attributed to the formation of an additional hydrogen bond in the ABL-7 and T315I-7 complexes. Thus, the differences in the structural and energetic features associated with the binding modes of 1 and 7 indicate that the hydrogen bonds with Met318 should be considered as the key interactions in designing the potent ABL inhibitors.

Consistent with a significant increase in the inhibitory activities for the wild type and T315I mutant, the ΔG_b^{aq} values of 28 are lower than those of 11 by 2.6 kcal/mol for the wild type and by 2.9 kcal/mol for T315I mutant. We note in this regard that the ΔG^{sol} value of 28 is 2.8 kcal/mol higher than that of 11 whereas the ΔG_b^{gas} values of the two inhibitors are similar for both receptors. This difference indicates that the substantially enhanced inhibitory activity because of the substitution of benzothiazole group in 28 for benzimidazole ring in 11 stems from the reduced desolvation cost for complexation rather than the strengthening of enzyme–inhibitor interactions. The comparable ΔG_b^{gas} values of 11 and 28 are actually not surprising because their calculated binding modes are similar for both the wild type and T315I mutant as shown in Figure 6. The large difference in ΔG^{sol} values of 11 and 28 can also be understood because imidazole is soluble a little in water while thiazole has only a micromolar water-solubility.⁴¹ Thus, the energetic features found in this study demonstrate that the potency of an inhibitor can be optimized by reducing the desolvation cost for enzyme–inhibitor complexation, as well as by strengthening the interactions between the inhibitor and the target protein. In contrast to more than 10-fold increase in the inhibitory activity because of the replacement of the terminal pyridine ring in 28 with 2-methoxyphenyl group in 29, the ΔG_b^{aq} values of 28 and 29 are predicted to be similar. This disagreement indicates that despite the improvement with the solvation term, the scoring function remains insufficient by itself to fully characterize the relative potencies of nocodazole derivatives.

MD Simulations. We attempted to identify the dynamic properties of enzyme–inhibitor complexes to elucidate the difference in inhibitory activities of 28 and 29 by conducting MD simulations of the wild type and T315I mutant of ABL in complex with 28 and 29. The dynamic stabilities of the wild type and T315I mutant in solution were evaluated by calculating the time evolutions of RMSD_{init} values of backbone C_α atoms from the starting structures of production dynamics

for ABL-28, T315I-28, ABL-29, and T315I-29 complexes. As shown in Figure 7a, the $\text{RMSD}_{\text{init}}$ values remain within 2.5 Å

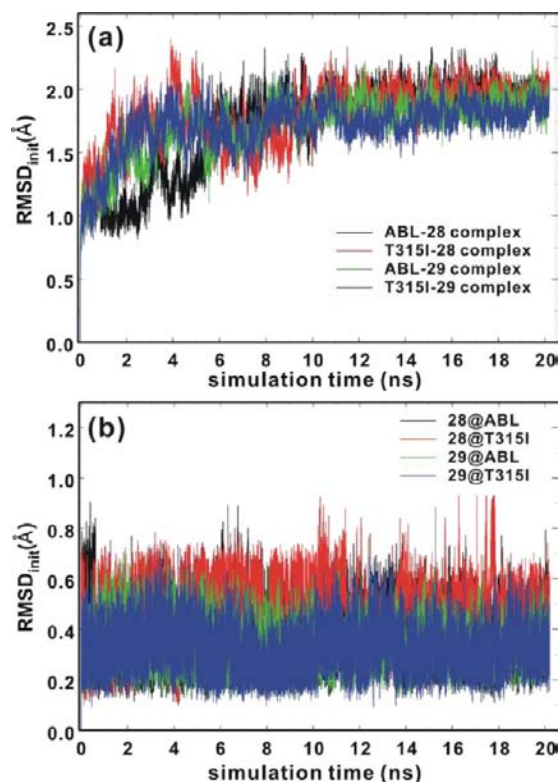


Figure 7. Time evolutions of $\text{RMSD}_{\text{init}}$ values of (a) protein backbone C_{α} atoms and (b) heavy atoms of **28** and **29** from the starting structures of production dynamics.

during the entire course of simulation in all four cases, exhibiting a convergent behavior with respect to the simulation time. These results indicate that the protein structures can be maintained stable in all four cases without a significant conformational change under the simulation conditions described above. It is also noteworthy that the $\text{RMSD}_{\text{init}}$ values for the heavy atoms of **28** and **29** fall into 1 Å and are maintained lower than those of C_{α} atoms of the wild type and T315I mutant of ABL throughout the entire simulation time (Figure 7b). This suggests that the movements of **28** and **29** within the ATP-binding sites are insignificant when compared to the conformational changes of the wild type and T315I mutant, which is consistent with their high inhibitory activities.

Because the hydrogen bond interactions with backbone groups of Met318 were found to be the most important interactions to stabilize the inhibitors in the ATP-binding sites of the wild type and T315I mutant, the difference in the inhibitory activities of **28** and **29** may be elucidated by comparing the dynamic properties of the three hydrogen bonds shown in Figure 6. Figure 8 displays the time dependences of the interatomic distances associated with the three hydrogen bonds. A common feature of ABL-**28**, T315I-**28**, ABL-**29**, and T315I-**29** complexes is that the central hydrogen bond established between the H2 atom of the inhibitors and the aminocarbonyl oxygen of Met318 is dynamically most stable with the time-averaged distances of 1.9–2.0 Å. This hydrogen bond is found to be preserved for more than 95% of simulation time in all four cases when the distance limit of N–H...O hydrogen bond is assumed to be 2.5 Å. The hydrogen bond between N1 atom of the inhibitors and amidic hydrogen of Met318 also exhibits a dynamic stability in all four enzyme–inhibitor complexes. It appears to be established for 94.2%, 93.9%, 92.4%, and 96.5% of residence time in ABL-**28**, T315I-**28**, ABL-**29**, and T315I-**29** complexes, respectively.

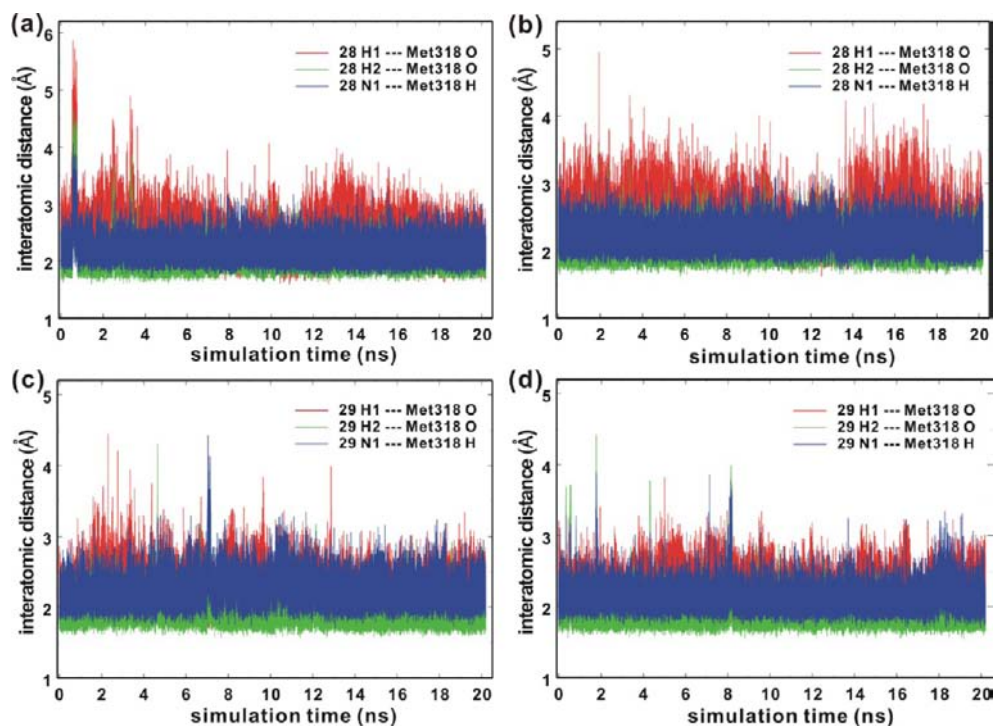


Figure 8. Time evolutions of the interatomic distances associated with the hydrogen bond interactions of **28** and **29** with backbone amide group of Met318 in (a) ABL-**28**, (b) T315I-**28**, (c) ABL-**29**, and (d) T315I-**29** complexes. See Figure 6 for the identification of atoms.

Table 3. Calculated Free Energy Changes in Solution (ΔG_u) and in the ATP-Binding Sites of Wild Type (WT) and T315I Mutant ABL (ΔG_b), and the Change in Binding Free Energies ($\Delta\Delta G_{\text{bind}}$) Associated with the Structural Transformation between the Two Structurally Similar Inhibitors^a

perturbation		1 → 7	9 → 11	11 → 28	28 → 29
ΔG_u		-7.3 ± 0.0	4.4 ± 0.5	1.3 ± 0.0	1.4 ± 0.3
ΔG_b	WT	-8.3 ± 0.0	5.1 ± 0.7	0.5 ± 0.0	-1.6 ± 0.4
	T315I	-8.6 ± 0.1	5.6 ± 1.1	0.5 ± 0.0	-1.3 ± 0.2
$\Delta\Delta G_{\text{bind}}$	WT	-1.0 ± 0.0	0.7 ± 0.9	-0.8 ± 0.0	-3.0 ± 0.5
	T315I	-1.3 ± 0.1	1.2 ± 1.2	-0.8 ± 0.0	-2.7 ± 0.4

^aAll energy values are given in kcal/mol.

Another common feature of the four enzyme–inhibitor complexes lies in the dynamic instability of the hydrogen bond between H1 atom of the inhibitors and the aminocarbonyl oxygen of Met318. This hydrogen bond is located at the entrance of the ATP-binding site and is exposed to bulk solvent, which allows the hydrogen bond to be ruptured by solvent molecules. It is found to be maintained only for 63.7 and 64.3% of simulation time in ABL-28 and T315I-28 complexes, respectively. However, the dynamic stability of the hydrogen bond increases significantly with the change of the inhibitor from 28 to 29. The H1...O=C hydrogen bonds are preserved for 85.6 and 87.8% of residence time in ABL-29 and T315I-29 complexes, respectively. Therefore, the higher inhibitory activity of 29 compared to 28 can be attributed to the strengthening of the hydrogen bond between H1 atom and the aminocarbonyl oxygen of Met318.

The higher dynamic stability of the hydrogen bonds between 29 and the wild type and T315I mutant of ABL than those for 28 can be understood by comparing the RMSD_{init} values of the inhibitors. As shown in Figure 7b, the RMSD_{init} values of 29 are dynamically more stable than those of 28 when bound to the ATP-binding site of the wild type and the mutant. The time-averaged RMSD_{init} values amount to only 0.32 and 0.30 Å for ABL-29 and T315I-29 complexes, as compared to 0.41 and 0.49 Å for ABL-28 and T315I-28 complexes, respectively. Therefore, 29 is expected to be motionally more restricted in the ATP-binding sites than 28. This indicates that 29 can be bound in the ATP binding sites more tightly than 28, which is consistent with the establishment of the stronger hydrogen bonds in ABL-29 and T315I-29 complexes than in ABL-28 and T315I-28 complexes. Thus, dynamic properties of enzyme–inhibitor complexes provide useful information for designing new potent inhibitors of the wild type and T315I mutant of ABL as well as the binding free energies and the binding modes estimated from docking simulations.

To further address the importance of the hydrogen bonds in the potencies of the inhibitors, we compare the binding free energies of ABL-29 and T315I-29 complexes including all three hydrogen bonds with those of ABL-28 and T315I-28 complexes in which only two hydrogen bonds are involved. For this purpose, additional docking simulations of 28 and 29 were carried out in the ATP-binding sites of the wild type and T315I mutant of ABL. As the starting structures, we used the MD trajectory snapshots for ABL-29 and T315I-29 complexes in which 29 formed all three hydrogen bonds with Met318 and those for ABL-28 and T315I-28 complexes in which one N–H...O hydrogen bond was broken. The calculated binding free energy appears to become more favorable from -12.1 to -13.0 kcal/mol in going from ABL-28 to ABL-29 complex. Similarly, T315I-29 complex is found to be more stable than T315I-28 complex by 1.3 kcal/mol because of the establishment of an

additional hydrogen bond with the backbone amide group of Met318. These results confirm the significant role of Met318 in the stabilizing the inhibitor through the formation of multiple hydrogen bonds. A similar result was also obtained in the molecular modeling studies reported by Cortopassi and coworkers.⁴²

FEP Calculations. Table 3 lists the calculated $\Delta\Delta G_{\text{bind}}$ values with respect to the wild type and T315I mutant of ABL between the two structurally similar nocodazole derivatives shown in Table 1. Consistent with more than 20-fold increase of the inhibitory activity in going from 1 to 7, the calculated binding free energy (ΔG_{bind}) values become more favorable in 1 → 7 perturbation by 1.0 and 1.3 kcal/mol with respect to the wild type and T315I mutant of ABL, respectively. Because ΔG_b is more negative than ΔG_u both for the wild type and for T315I mutant, the increase of inhibitor potency in going from 1 to 7 can be attributed to the greater stabilization in the ATP-binding sites than in solution with the change of the terminal methoxy group in 1 to the ethylamine moiety in 7. This result also indicates that to enhance the inhibitory activity, the structural modification of an inhibitor should be made in such a way for the strengthening of enzyme–inhibitor interactions to over-balance the extra stabilization of the new inhibitor in solution.

In case of 9 → 11 perturbation, $\Delta\Delta G_{\text{bind}}$ values become unpredictable within the framework of FEP theory because of the large statistical errors in both ΔG_u and ΔG_b . We note in this regard that the two terminal methoxy moieties in 9 should disappear in 11 with the additional change of a carbon on the terminal phenyl ring to a nitrogen atom. Such a structural variation seems to be too large to be described properly by FEP calculations. On the other hand, all statistical errors fall into 0.05 kcal/mol in 11 → 28 FEP calculations. In this case the magnitudes of ΔG_u and ΔG_b are also found to be smallest among the four perturbations under consideration, which is not surprising because the structural transformation of 11 into 28 involves only the change of the -NH- group on the benzimidazole ring to a sulfur atom. The more positive value of ΔG_u than ΔG_b in 11 → 28 perturbation implies that the inhibitor can become more potent because it is less destabilized in the ATP-binding sites than in aqueous solution. This result exemplifies the importance of reducing the desolation cost for enzyme–inhibitor complexation to improve the inhibitor potency, which is consistent with the decomposition analysis of binding free energies in Table 2.

The results of 28 → 29 FEP calculations differ from those of binding free energy decomposition analysis in that ΔG_u and ΔG_b values become positive and negative, respectively, as 28 transforms into 29. This indicates that the resulting improvement of inhibitory activity can be attributed to the combined effects of the destabilization of the inhibitor in bulk solvent and the stabilization of the enzyme–inhibitor complex. Thus, the

results of FEP calculations for nocodazole derivatives confirm that the enhancement of inhibitor potency can be achieved by the reduction of the desolvation cost for enzyme–inhibitor complexation, as well as by the strengthening of the interactions between the inhibitor and the amino-acid residues in the ATP-binding site.

CONCLUSIONS

We have identified new common inhibitors of the wild-type and T315I mutant of ABL by applying a structure-based de novo design using nocodazole as the inhibitor scaffold. Because of the improvement of the scoring function by implementing a proper solvation free energy term, the majority of the designed derivatives are found to have a higher potency than nocodazole. In particular, compound 29 reveals picomolar inhibitory activity against both the wild type and T315I mutant, indicating that it may serve as a new lead compound for the discovery of anti-CML drugs. Decomposition analysis of the binding free energies indicates that in order to enhance the potency of an ABL inhibitor with structural modifications, the strengthening of enzyme–inhibitor interactions should be greater than the increase in desolvation cost for binding in the ATP-binding site. Consistent with the previous experimental and computational studies, the hydrogen bond interactions with backbone groups of Met318 are found to be the most significant binding forces associated with the stabilization the inhibitors in the ATP-binding sites of the wild type and T315I mutant. Besides the strength of the hydrogen bonds with Met318, dynamic stabilities of the hydrogen bonds appear to be also important for the effective inhibition of the wild type and T315I mutant of ABL. The results of FEP calculations for nocodazole derivatives confirm that the inhibitory activity can be enhanced not only by the strengthening of the binding in the ATP-binding site but also by the reduction of the desolvation cost for enzyme–inhibitor complexation.

ASSOCIATED CONTENT

Supporting Information

Experimental procedures, characterization data, and copies of ^1H and ^{13}C NMR spectra for all compounds. This material is available free of charge via the Internet at <http://pubs.acs.org>.

AUTHOR INFORMATION

Corresponding Author

hspark@sejong.ac.kr; hongorg@kaist.ac.kr

Notes

The authors declare no competing financial interest.

ACKNOWLEDGMENTS

Dedicated to Professor Deukjoon Kim on the occasion of his retirement. This research was supported by National Research Foundation of Korea (NRF) funded by the Ministry of Education, Science and Technology (NRF-2012-0008440, 2011-0016436, 2011-0020322) and the Institute for Basic Science (IBS).

REFERENCES

- (1) Quintas-Cardama, A.; Cortes, J. *Blood* **2009**, *113*, 1619.
- (2) Eck, M. J.; Manley, P. W. *Curr. Opin. Cell Biol.* **2009**, *21*, 288.
- (3) Schenone, S.; Bruno, O.; Radi, M.; Botta, M. *Med. Res. Rev.* **2010**, *31*, 1.

(4) Capdeville, R.; Buchdunger, E.; Zimmermann, J.; Matter, A. *Nat. Rev. Drug Discov.* **2002**, *1*, 493.

(5) O'Hare, T.; Eide, C. A.; Deininger, M. W. *Blood* **2007**, *110*, 2242.

(6) Quintas-Cardama, A.; Kantarjian, H.; Cortes, J. *Nat. Rev. Drug Discovery* **2007**, *6*, 834.

(7) Lombardo, L. J.; Lee, F. Y.; Chen, P.; Norris, D.; Barrish, J. C.; Behnia, K.; Castaneda, S.; Cornelius, L. A. M.; Das, J.; Doweiko, A. M.; Fairchild, C.; Hunt, J. T.; Inigo, I.; Johnston, K.; Kamath, A.; Kan, D.; Klei, H.; Marathe, P.; Pang, S.; Peterson, R.; Pitt, S.; Schieven, G. L.; Schmidt, R. J.; Tokarski, J.; Wen, M. L.; Wityak, J.; Borzilleri, R. M. *J. Med. Chem.* **2004**, *47*, 6658.

(8) Weisberg, E.; Manley, P. W.; Breitenstein, W.; Brügger, J.; Cowan-Jacob, S. W.; Ray, A.; Huntly, B.; Fabbro, D.; Fendrich, G.; Hall-Meyers, E.; Kung, A. L.; Mestan, J.; Daley, G. Q.; Callahan, L.; Catley, L.; Cavazza, C.; Azam, M.; Neuberg, D.; Wright, R. D.; Gilliland, D. G.; Griffin, J. D. *Cancer Cell* **2005**, *7*, 129.

(9) Kimura, S.; Naito, H.; Segawa, H.; Kuroda, J.; Yuasa, T.; Sato, K.; Yokota, A.; Kamitsuji, Y.; Kawata, E.; Ashihara, E.; Nakaya, Y.; Naruoka, H.; Wakayama, T.; Nasu, K.; Asaki, T.; Niwa, T.; Hirabayashi, K.; Maekawa, T. *Blood* **2005**, *106*, 3948.

(10) Boschelli, D. H.; Ye, F.; Wang, Y. D.; Dutia, M.; Johnson, S. L.; Wu, B.; Miller, K.; Powell, D. W.; Yaczko, D.; Young, M.; Tischler, M.; Arndt, K.; Discafani, C.; Etienne, C.; Gibbons, J.; Grod, J.; Lucas, J.; Weber, J. M.; Boschelli, F. *J. Med. Chem.* **2001**, *44*, 3965.

(11) Zhou, T.; Parillon, L.; Li, F.; Wang, Y.; Keats, J.; Lamore, S.; Xu, Q.; Shakespeare, W.; Dalgarno, D.; Zhu, X. *Chem. Biol. Drug Des.* **2007**, *70*, 171.

(12) Giles, F. J.; Cortes, J.; Jones, D.; Bergstrom, D.; Kantarjian, H.; Freedman, S. J. *Blood* **2007**, *109*, 500.

(13) Gontarewicz, A.; Balabanov, S.; Keller, G.; Colombo, R.; Graziano, A.; Pesenti, E.; Bente, D.; Bokemeyer, C.; Fiedler, W.; Moll, J.; Brümmendorf, T. H. *Blood* **2008**, *111*, 4355.

(14) Howard, S.; Berdini, V.; Boulstridge, J. A.; Carr, M. G.; Cross, D. M.; Curry, J.; Devine, L. A.; Early, T. R.; Fazal, L.; Gill, A. L.; Heathcote, M.; Maman, S.; Matthews, J. E.; McMenamin, R. L.; Navarro, E. F.; O'Brien, M. A.; O'Reilly, M.; Rees, D. C.; Reule, M.; Tisi, D.; Williams, G.; Vinković, M.; Wyatt, P. G. *J. Med. Chem.* **2009**, *52*, 379.

(15) Shiotsu, Y.; Kiyoi, H.; Ishikawa, Y.; Tanizaki, R.; Shimizu, M.; Umehara, H.; Ishii, K.; Mori, Y.; Ozeki, K.; Minami, Y.; Abe, A.; Maeda, H.; Akiyama, T.; Kanda, Y.; Sato, Y.; Akinaga, S.; Naoue, T. *Blood* **2009**, *114*, 1607.

(16) Quintas-Cardama, A.; Cortes, J. *Clin. Cancer Res.* **2008**, *14*, 4392.

(17) (a) Park, H.; Hong, S.; Hong, S. *J. Comput.-Aided Mol. Des.* **2012**, *26*, 983. (b) Choi, H. G.; Ren, P.; Adrian, F.; Sun, F.; Lee, H. S.; Wang, X.; Ding, Q.; Zhang, G.; Xie, Y.; Zhang, J.; Liu, Y.; Tuntland, T.; Warmuth, M.; Manley, P. W.; Mestan, J.; Gray, N. S.; Sim, T. *J. Med. Chem.* **2010**, *53*, 5439. (c) Huang, W. S.; Metcalf, C. A.; Sundaramoorthi, R.; Wang, Y.; Zou, D.; Thomas, R. M.; Zhu, X.; Cai, L.; Wen, D.; Liu, S.; Romero, J.; Qi, J.; Chen, I.; Banda, G.; Lentini, S. P.; Das, S.; Xu, Q.; Keats, J.; Wang, F.; Wardwell, S.; Ning, Y.; Snodgrass, J. T.; Broudy, M. I.; Russian, K.; Zhou, T.; Commodore, L.; Narasimhan, N. I.; Mohemmad, Q. K.; Iulucci, J.; Rivera, V. M.; Dalgarno, D. C.; Sawyer, T. K.; Clackson, T.; Shakespeare, W. C. *J. Med. Chem.* **2010**, *53*, 4701. (d) Thomas, M.; Huang, W. S.; Wen, D.; Zhu, X.; Wang, Y.; Metcalf, C. A.; Liu, S.; Chen, I.; Romero, J.; Zou, D.; Sundaramoorthi, R.; Li, F.; Qi, J.; Cai, L.; Zhou, T.; Commodore, L.; Xu, Q.; Keats, J.; Wang, F.; Wardwell, S.; Ning, Y.; Snodgrass, J. T.; Broudy, M. I.; Russian, K.; Iulucci, J.; Rivera, V. M.; Sawyer, T. K.; Dalgarno, D. C.; Clackson, T.; Shakespeare, W. C. *Bioorg. Med. Chem. Lett.* **2011**, *21*, 3743. (e) Deng, X.; Lim, S. M.; Zhang, J.; Gray, N. S. *Bioorg. Med. Chem. Lett.* **2010**, *20*, 4196. (f) Cao, J.; Fine, R.; Gritzen, C.; Hood, J.; Kang, X.; Klebansky, B.; Lohse, D.; Mak, C. C.; McPherson, A.; Noronha, G.; Palanki, M. S. S.; Pathak, V. P.; Renick, J.; Soll, R.; Zeng, B.; Zhu, H. *Bioorg. Med. Chem. Lett.* **2007**, *17*, 5812.

(18) (a) Gambacorti-Passerini, C.; Gasser, M.; Ahmed, S.; Assouline, S.; Scapozza, L. *Leukemia* **2005**, *19*, 1267. (b) Lü, S.; Luo, Q.; Hao, X.; Li, X.; Ji, L.; Zheng, W.; Wang, F. *Bioorg. Med. Chem. Lett.* **2011**, *21*, 6964. (c) Wang, D.; Zhang, Z.; Lu, X.; Feng, Y.; Luo, K.; Gan, J.

Yingxue, L.; Wan, J.; Li, X.; Zhang, F.; Tu, Z.; Cai, Q.; Ren, X.; Ding, K. *Bioorg. Med. Chem. Lett.* **2011**, *21*, 1965.

- (19) Park, H.; Hong, S.; Hong, S. *ChemMedChem* **2012**, *7*, 53.
- (20) Warren, G. L.; Andrews, C. W.; Capelli, A. M.; Clarke, B.; LaLonde, J.; Lambert, M. H.; Lindvall, M.; Nevins, N.; Semus, S. F.; Senger, S.; Tedesco, G.; Wall, I. D.; Woolven, J. M.; Peishoff, C. E.; Head, M. S. *J. Med. Chem.* **2006**, *49*, 5912.
- (21) Shoichet, B. K.; Leach, A. R.; Kuntz, I. D. *Proteins* **1999**, *34*, 4.
- (22) Tokarski, J. S.; Newitt, J. A.; Chang, C. Y. J.; Cheng, J. D.; Wittekind, M.; Kiefer, S. E.; Kish, K.; Lee, F. Y. F.; Borzillerri, R.; Lombardo, L. J.; Xie, D.; Zhang, Y.; Klei, H. E. *Cancer Res.* **2006**, *66*, 5790.
- (23) Jeffrey, G. A. *An Introduction to Hydrogen Bonding*; Oxford University Press: Oxford, U.K., 1997.
- (24) Wang, R.; Gao, Y.; Lai, L. *J. Mol. Model.* **2000**, *6*, 498.
- (25) Wang, R.; Liu, L.; Lai, L. *J. Mol. Model.* **1998**, *6*, 379.
- (26) Lipinski, C. A.; Lombardo, F.; Dominy, B. W.; Feeney, P. J. *Adv. Drug Delivery Rev.* **1997**, *23*, 3.
- (27) Morris, G. M.; Goodsell, D. S.; Halliday, R. S.; Huey, R.; Hart, W. E.; Belew, R. K.; Olson, A. J. *J. Comput. Chem.* **1998**, *19*, 1639.
- (28) Park, H.; Jeon, J. H. *Phys. Rev. E* **2007**, *75*, 021916.
- (29) Gasteiger, J.; Marsili, M. *Tetrahedron* **1980**, *36*, 3219.
- (30) Stouten, P. F. W.; Frömmel, C.; Nakamura, H.; Sander, C. *Mol. Simul.* **1993**, *10*, 97.
- (31) Choi, H.; Kang, H.; Park, H. *J. Cheminformatics* **2013**, *5*, 8.
- (32) Park, H.; Chi, O.; Kim, J.; Hong, S. *J. Chem. Inf. Model.* **2011**, *51*, 2986.
- (33) The IC₅₀ determinations were performed at the Reaction Biology Corp. See the Supporting Information for details.
- (34) Case, D. A.; Cheatham, T. E., III; Darden, T.; Gohlke, H.; Luo, R.; Merz, K. M., Jr.; Onufriev, A.; Simmerling, C.; Wang, B.; Woods, R. *J. J. Comput. Chem.* **2005**, *26*, 1668.
- (35) Fox, T.; Kollman, P. A. *J. Phys. Chem. B* **1998**, *102*, 8070.
- (36) Jorgensen, W. L.; Chandrasekhar, J.; Madura, J. D.; Impey, R. W.; Klein, M. L. *J. Chem. Phys.* **1983**, *79*, 926.
- (37) Berendsen, H. J. C.; Postma, J. P. M.; van Gunsteren, W. F.; DiNola, A.; Haak, J. R. *J. Chem. Phys.* **1984**, *81*, 3684.
- (38) Ryckaert, J.-P.; Ciccotti, G.; Berendsen, H. J. C. *J. Comput. Phys.* **1977**, *23*, 327.
- (39) O'Hare, T.; Heide, C. A.; Deininger, M. W. *Expert Opin. Invest. Drugs* **2008**, *17*, 865.
- (40) Levinson, N. M.; Boxer, S. G. *PLoS One* **2012**, *7*, e29828.
- (41) Li, C.-M.; Chen, J.; Lu, Y.; Narayanan, R.; Parke, D. N.; Li, W.; Ahn, S.; Miller, D. D.; Dalton, J. T. *Drug Metab. Dispos.* **2011**, *39*, 1833.
- (42) Cortopassi, W. A.; Feital, R. J. C.; Medeiros, D. J.; Guizado, T. R. C.; França, T. C. C.; Pimentel, A. S. *Mol. Simul.* **2012**, *38*, 1132.